Journal of Applied Polymer Science

Fabrication of super-ductile PP/LDPE blended parts with a chemical blowing agent

Ying-Guo Zhou,[1] Bei Su,[1] Lih-Sheng Turng[2,3]

[1]Department of Materials and Forming, School of Material Science and Engineering, Jiangsu University of Science and Technology, Zhenjiang Jiangsu 212003, People's Republic of China

[2]Department of Mechanical Engineering, Polymer Engineering Center, University of Wisconsin-Madison, Madison, 53706

[3]Department of BIONATES, Wisconsin Institute for Discovery, University of Wisconsin-Madison, Madison, 53715

Correspondence to: Y.-G. Zhou (E-mail: zhouyingguo@gmail.com) and L.-S. Turng (E-mail: turng@engr.wisc.edu)

ABSTRACT: The mechanical blending of polypropylene (PP) and low density polyethylene (LDPE) is an economical and simple method for producing new polymeric materials for specific applications. However, the reduction in strain-at-break of the blend is one of its main shortcomings. In this study, PP/LDPE foamed parts were fabricated by conventional injection molding (CIM) with azodicarbonamide as a chemical blowing agent (CBA) and tested for tensile properties at two test speeds. Also, the fracture surfaces of the parts were investigated by scanning electron microscopy (SEM). In addition, to investigate the underlying mechanism of the super-ductility, the tested samples were carefully analyzed and compared, and further characterized by differential scanning calorimetry and SEM. The results suggest that fabricating PP/LDPE super-ductile parts using CIM with a CBA is feasible. The results also indicate that there is a close relationship between the mechanical properties and morphological structures, which are deeply influenced by the dosage of CBA, the PP/LDPE ratio, and the packing parameters. Furthermore, compared to conventional injection molded solid parts, the ductility of the foamed parts can be dramatically improved by the formation of microfibrils in the PP phase, which come into being under certain processing conditions. © 2016 Wiley Periodicals, Inc. J. Appl. Polym. Sci. **2016**, *133*, 44101.

KEYWORDS: foams; injection molding; properties and characterization; structure-property relations

Received 29 February 2016; accepted 19 June 2016
DOI: 10.1002/app.44101

INTRODUCTION

Polypropylene (PP) and low density polyethylene (LDPE) are both widely used thermoplastic resins owing to their advantages such as low density, low cost, and easy processing. The mechanical blending of PP and LDPE, if they result in an improved product, may prove to be a more economical and easier method for producing new polymeric materials for specific applications.[1–3] In the past decade, high volume commodity PP and LDPE have been blended in hopes of combining the mechanical performance of both components.[4–8] Furthermore, with their more similar chemical structures, the possibility of recycling plastic waste—mainly constituted by polyolefins[9,10]—and avoiding the complex and expensive processes of separation of the different components has been investigated. Generally, blending PP and PE yields properties in- between those of the original homopolymers. However, the main shortcoming of the blends is the drastic reduction in elongation-at-break.[4,5] Hence, for the successful application of PP/LDPE blends, improvement in elongation-at-break is important.

Similar to other common toughness-enhancing methods, to enhance the ductility or toughness of a component fabricated by PP/LDPE blends, one can introduce microparticles or nanoparticles—such as talc, nanoclay, nanoSiO_2, cellulose nanofibers, or elastomeric core–shell particles—into the blended material.[11–18] In addition, it has been proven that LDPE and PP are incompatible in the melt and the blend exists as a two-phase mixture.[19] Therefore, the poor interfacial bond strength between both phases can explain the weak mechanical properties that are directly linked to the blend's morphology.[20] Many studies have been published concerning the improvement of the mechanical performance by adding compatibilizers[21] such as styrene-butadiene-styrene,[22] ethylene-propylene-diene rubber,[23] ethylene-propylene-ethylidene norborene copolymer (EPCAR-847),[24] and PE-g-poly(2-methyl-1,3-butadiene).[9]

Recently, a novel ductility-enhancing method was proposed by Sun et al.[25,26] They found that improvements in part ductility and toughness could be achieved by creating a microcellular foam structure using microcellular injection molding in PP/

LDPE blends. A dramatic increase in the ductility of PP/LDPE microcellular parts was investigated and compared to solid parts. In general, foamed plastic parts offer a number of advantages to molders and end-users. For example, introducing gas or air bubbles into a polymer can reduce costs from lower resin consumption, insulation, shock absorption, reduced part weight, and decreased molding pressures and part shrinkage.[27] However, it is unlikely that the mechanical performance of fabricated foamed parts can exceed that of their solid counterparts. If foamed plastic parts can provide good physical performance, it is beyond all doubt that polymeric foamed components will become an increasingly more important part of polymer production. As a result, PP/LDPE blends will be used more widely, especially with their improved ductility.

One major issue with the aforementioned method is that a physical blowing agent (PBA) delivery and dosing system are required and need to be specially designed. Regarding the nature of the foaming process, there are, in general, two categories: physical foaming and chemical foaming. In the physical foaming process, the polymer and a PBA are first made into a uniform mixture.[28,29] When the temperature change is applied, the solubility and miscibility of these two components with each other are reduced. As a result, phase change and phase separation are induced, which leads to a cell nucleation and growth process. There are many kinds of PBAs that have been successfully applied in this process, and the representative ones are CO_2 and N_2. Conversely, the chemical foaming process is driven by a chemical reaction of a chemical blowing agent (CBA) incorporated into a polymer.[30,31] The CBA is thermally unstable and will decompose or dissolve during the processing stage of the process used—for example, extrusion or injection molding—yielding one or more gases such as CO_2 and N_2 to initiate the cell nucleation process and sustain cell growth.

Compared to the equipment costs of PBAs, almost all CBAs are solid, and no special storage or handling equipment is required. This motivated us to explore other methods of improving the ductility of PP/LDPE blends using CBAs. However, the use of CBAs does not allow for good control over the foaming process or the porosity and cellular structure of the parts.[32] As a result, a careful investigation of the processing conditions and foaming structure needed to be carried out. In our previous work, a novel method for improving toughness and enhancing ductility using a CBA was proposed.[33] This method produced lightweight injection molded parts with improved elongation as compared to their solid counterparts. Meanwhile, no special storage, delivery, or handling equipment was needed. In this study, a method was introduced and the results were carefully compared. A better understanding of the ductility-enhancing mechanism was gained from the results and from comparisons with conventional injection molded parts.

EXPERIMENTAL

Materials

The PP (T30S) used in this study was a commercial product made in China. Its melt flow index was about 3.2 g/10 min (190 °C, 21.6 N). LDPE (951-000) was purchased from China. It had a melt flow index of 2.17 g/10 min (230 °C, 21.6 N). The

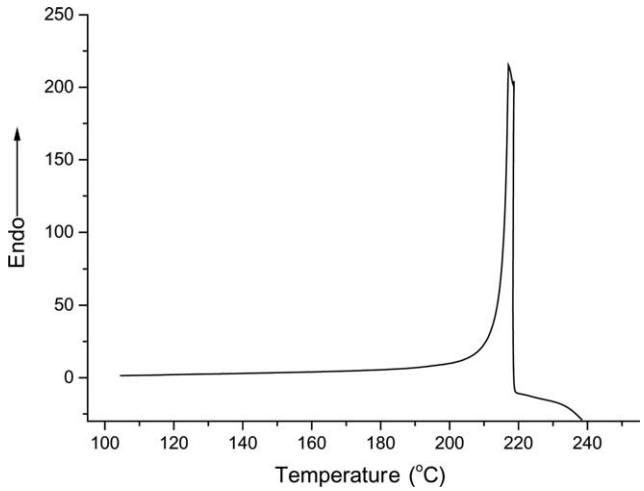

Figure 1. The heating flow curve of AC used at a heating rate of 10 °C/min.

CBA used was azodicarbonamide (AC) and its type was Dn8. The thermal decomposition behavior of this CBA was characterized and is shown in Figure 1 using a differential scanning calorimetry (DSC) test with a scan rate of 10 °C/min. As shown in Figure 1, its decomposition temperature was in the range of 193 to 218 °C, with a peak maximum at about 215 °C and a peak width of about 10 °C. The gases released during decomposition were N_2 (65%), CO (25%), CO_2 (5%), and NH_3 (5%). Residual solid decomposition products included urazol, biurea, cyamelide, and cyanuric acid. In this study, the CBA content in the material formulation varied between 0.5 and 2.0 wt %.

Sample Preparation

Sample preparation was realized in a two-step process. First, AC and PP were mixed into the molten LDPE material during the extrusion process. The weight ratio of AC:LDPE and PP:LDPE varied across a range of 1:5–50 and 1:1–5, respectively, depending on the process used. The extruded material was cooled down at a moderate rate and then pelletized. The temperature of the extruder was set as low as 165 °C to avoid the decomposition of AC when the AC/LDPE was extruded. Regarding the PP/LPDE blend, the temperature was fixed at 170 °C in this study. The AC/LDPE and PP/LDPE were then mixed at a weight ratio of 1:19–39. As a result, the AC content in the PP/LDPE/AC composite was 0.5–2%. Using solid injection molding for comparison, there were six AC sample formulations by weight: 0, 0.5, 0.6, 0.8, 1.0, and 2.0%, respectively. In addition, nine kinds of compositions of PP/LDPE were selected for investigation in the study; namely, PL01, PL13, PL12, PL11, PL21, PL31, PL41, PL51, and PL10, where P and L denote PP and LDPE, respectively, and the subsequent numbers denote the weight ratio of PP/LDPE; that is, 01 means the ratio is 0:1, 11 means the ratio is 1:1, and so forth.

The next step was to use the different PP/LDPE composites in a conventional injection molding (CIM) machine. It is well known that injection molded product defects such as warpage, shrinkage, and sink marks are caused by many factors during the production process. These defects influence the quality and dimensional accuracy of the products. Therefore, it is of critical

importance to effectively control these factors during the molding procedure. The processing parameters during CIM mainly include the melt temperature, mold temperature, injection pressure, injection time (rate), packing time, packing pressure, and cooling time. The packing pressure and/or time are often viewed as some of the most important factors.[34]

It should be noted that it is not easy to fabricate foamed parts with a CIM machine, especially micro-foamed parts. As the composite contains AC, once the composite is melted and blended in the CIM barrel under high temperature and pressure, a single-phase polymer–gas solution will form. As soon as this solution is injected into the mold cavity, it will create foamed injection molded parts due to cell nucleation, which is induced by the sudden pressure drop and sharp decrease of gas solubility in the polymer via a mechanism similar to microcellular injection molding. An appropriate range of temperatures and times needs to be set because the AC will decompose very rapidly once the temperature increases, and decomposition will slow or even stop when the temperature decreases. As a result, if the melt temperature is too high or the residence time is too long, the polymer–gas will seep through the nozzle of the CIM machine and drool directly into the mold sprue once the mold opens because of the pressure increase as the AC decomposes in the injection barrel of the machine. Conversely, if the temperature and/or time are not enough, the AC will not decompose completely. The foaming effect will be poor and the manufactured sample will be yellow due to the remaining AC.

In our study, we found that it was almost impossible to obtain the right balance of temperature and time in every injection molding operation using a CIM machine. In a CIM operation, the blended material is placed into the hopper of the CIM machine. It goes from the posterior end of the barrel to the jet nozzle as the process progresses, and 4–5 operation circles are often needed. The AC unavoidably decomposes during this interval of time. In this study, a method of "feeding and then injecting" was adopted to resolve this issue. That is, the material was fed separately for each cycle. The subsequent material goes into the hopper and is then converted into the polymer–gas melt with the rotation of the screw once the previous material has been injected into the mold. Although this procedure seems to be more complex, it has proven to be effective.

Based on the above "feeding and then injection" method, after many tests, the optimal processing parameters were obtained as follows: injection machine melt temperature of 200 °C, mold temperature of 50 °C, injection pressure of 50 MPa, injection time of 1 s, and cooling time of 20 s. Regarding the packing time and pressure, which will be discussed in detail in Influence of Packing Pressure and Time section, their optimized results were 1 s and 10 MPa, respectively. For the solid specimens, the packing pressure was fixed at 50 MPa and the packing time was 3 s. A standard tensile test bar mold was used to mold the parts, and its temperature was controlled by circulating oil from a thermal controller. The volume of the cavity was about 9.582×10^3 mm^3 and a detailed description of the molded sample is shown in Figure 2.

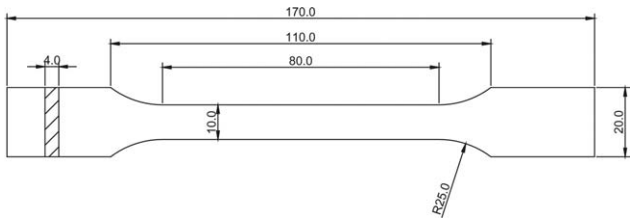

Figure 2. A detailed description of the molded sample. Units are in millimeters.

Sample Tests

The molded tensile bars were tested on a screw-driven universal testing instrument (MTS, Sintech 10/GL) per ASTM D638-03 at room conditions. Two crosshead speeds, 10 mm/min and 500 mm/min, were used to study the stress and strain behavior. At each test speed, at least five tensile bars were tested for each material and the mean and range of the modulus of elasticity (Young's modulus), ultimate tensile strength, and strain-at-break for each sample were calculated. In this study, the nominal tensile strength was obtained by dividing the maximum load by the original cross-sectional area.

The morphologies of the selected molded specimens were examined using a scanning electron microscope (SEM JEOL JSM-5000) with an accelerating voltage of 20 kV. The scanning electron microscopy (SEM) specimens were taken from the cross-section at the middle of the molded tensile bar that was fractured in liquid nitrogen. The surfaces of the fractured specimens were sputter coated with gold prior to observation.

A Perkin–Elmer DSC-8000 apparatus was used to analyze the thermal properties of the selected samples with a series of complex procedures. The DSC tests can be classified into two groups. The first group is related to the PP/LDPE composites with different amounts of PP. The samples were heated to 240 °C and kept at this temperature for 3 min to eliminate any residual crystals and prior thermomechanical history. Then they were cooled to 60 °C and kept for 3 min. Finally, the samples were reheated to 240 °C. For brevity, all of the heating/cooling rates were fixed at 10 °C/min. Sample weights were strictly limited in the range of 4.9–5.1 mg to avoid the possible influence of sample size. Samples were then crimped in aluminum pans loaded at 25 °C under a nitrogen atmosphere.

Generally, the slices were cut from the middle of the selected molded samples in these tests. However, the samples in the second group were specially selected. The upper part of the ruptured fibers formed by the tensile test and the topmost part of the threadlets (small thread- or hair-like protrusions) formed at the surface of the tensile tested samples were analyzed. The samples in this group underwent two heating/cooling cycles; they were heated to 165 °C first and then held for 3 min. Next they were cooled to 60 °C and held for 3 min. At the end of the first heating/cooling cycle, the samples were reheated to 220 °C, held for 3 min, and then cooled to room temperature. The DSC results for the two groups will be presented in the section below.

RESULTS AND DISCUSSION

Comparison among Injection Molded Samples

Influence of AC Content. Following References 18 and 19, the weight ratio of PP/LDPE was initially fixed at 3:1. The foamed

Figure 3. Pictures of the molded sample with different amounts of AC before and after the tensile test. The first one (a′) is the untested sample; the others (b′∼g′) are tested samples. From top to bottom, the AC content by weight was 0.6%, 0%, 0.5%, 0.6%, 0.8%, 1.0%, and 2.0%. The length of the ruler is 60 cm. [Color figure can be viewed in the online issue, which is available at wileyonlinelibrary.com.]

samples were prepared by CIM with the five typical amounts of AC by weight; that is, 0.5, 0.6, 0.8, 1.0, and 2.0%, respectively. For comparison, solid samples were prepared with the same thermal-mechanical history of the foamed parts but without AC and with different packing conditions. Recall that for the solid specimens, the packing pressure was fixed at 50 MPa and the packing time was 3 s. The weight of each sample was measured using a high precision scale with a maximum weight capacity of 500 g and a precision of 0.001 g. In this study, the average weights of the five groups of foamed samples were 7.710, 7.692, 7.656, 7.601, and 7.412 g, respectively, resulting in a weight reduction of 6–10% compared to the solid parts weighing 8.219 g.

Tensile tests were performed on the injection molded solid and foamed specimens of PP/LDPE blends. Properties such as the strength, modulus, and strain-at break were measured. The properties reported here are the actual readings measured for the solid and foamed specimens without taking into account the weight reduction of the foamed specimens. Figure 3 shows an illustrative comparison of the ductility of the molded samples. For the solid parts—those with an AC content of 0%—yielding and then necking were observed to occur. However, the necking only lasted a short distance, and then the part ruptured. For the foamed parts where the AC content was 0.6%, the necking spread throughout the gauge length and measured several hundred percent strain. This deformation behavior is similar to typical semi-crystalline polymers capable of undergoing chain orientation.[35] An interesting phenomenon can also be observed from Figure 3 in that a lot of threadlets (small thread- or hair-

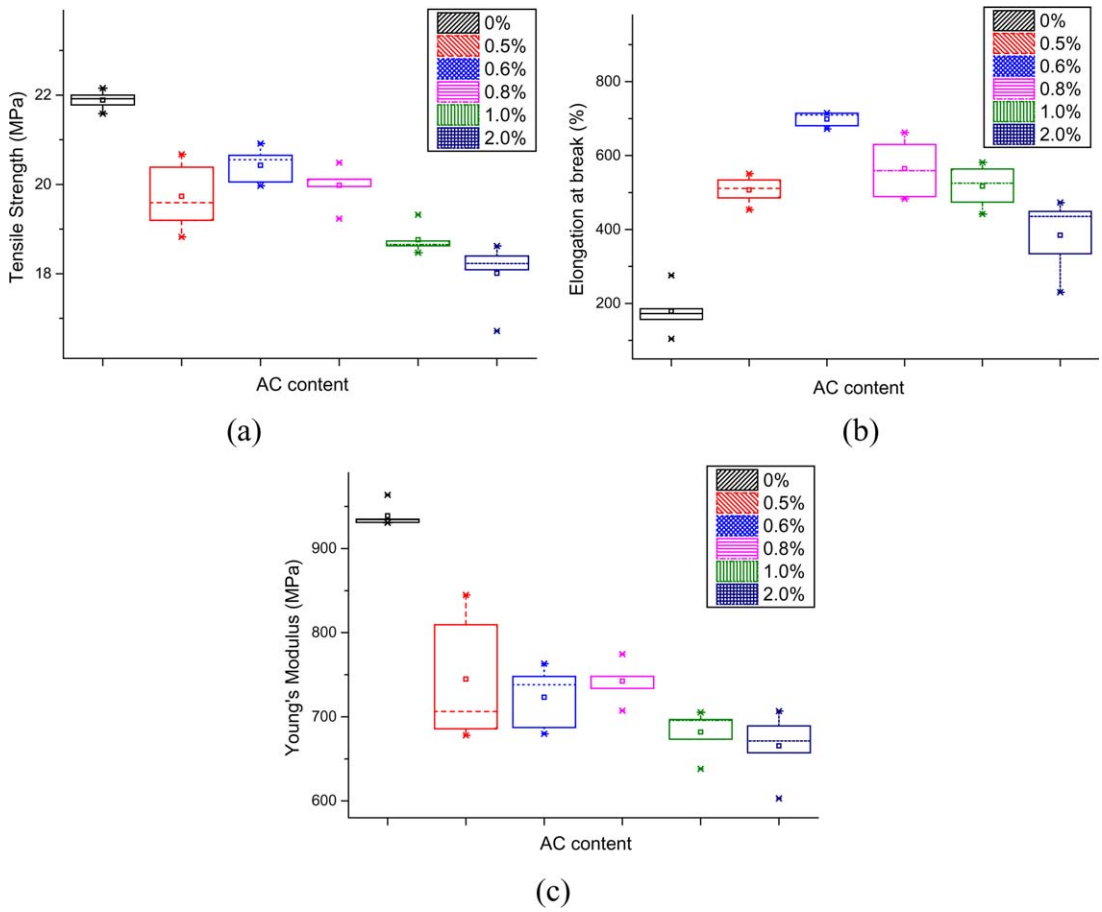

Figure 4. The (a) tensile strength, (b) strain-at-break, and (c) Young's modulus of the molded sample with different amounts of AC (tensile rate of 10 mm/min). [Color figure can be viewed in the online issue, which is available at wileyonlinelibrary.com.]

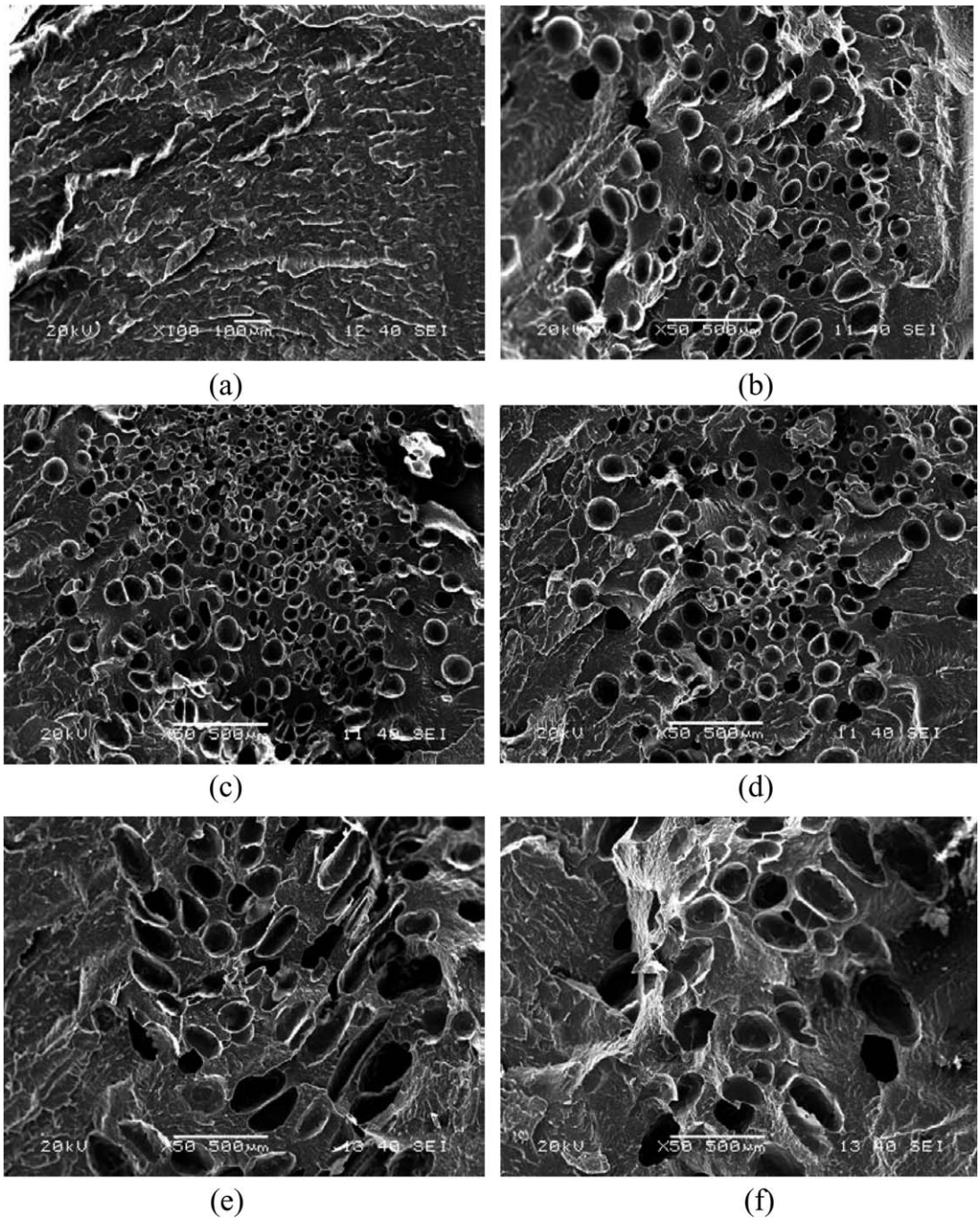

Figure 5. SEM images of the molded sample. The AC content by weight was (a) 0%, (b) 0.5%, (c) 0.6%, (d) 0.8%, (e) 1.0%, and (f) 2.0%, respectively.

like protrusions) formed on the surface of the samples with 0.5–0.8% AC content. The more ductility the sample had, the rougher the surface was, and the more threadlets that were found.

Figure 4 shows the results of tensile strength, strain-at-break, and moduli of the samples at a test speed of 10 mm/min with different amounts of AC. It can be seen from the figure that the foamed samples had a better strain-at-break than the solid ones, although their tensile strengths and Young's moduli were lower than the solid parts. With an increase in AC content, the tensile strengths and Young's moduli of the foamed samples obviously decreased. This result was not unexpected and could be attributed to the weight decrease. However, the strain-at-break of the foamed samples showed a strange trend with an increase in AC content. The best result of the strain-at-break occurred when the AC content was about 0.6% and showed approximately 700% strain-at-break. Once the AC content fell below or exceeded 0.6% AC content, the strain-at-break decreased and the experimental error increased. It is possible that the large

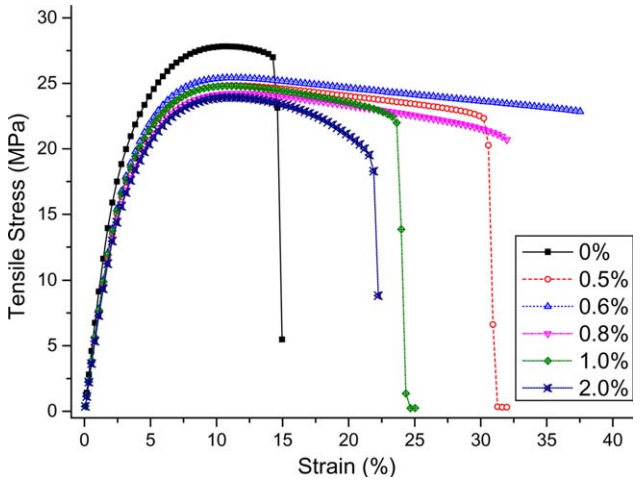

Figure 6. Tensile stress versus strain of the molded sample with different amounts of AC (tensile rate of 500 mm/min). [Color figure can be viewed in the online issue, which is available at wileyonlinelibrary.com.]

experimental error in the tensile test could be attributed to the foams not being uniformly distributed enough to show stable stress–strain behavior in the foamed sample.

The SEM is the most popular way to identify micro-structural changes of micro-foamed parts. SEM images provide information on the microstructure, including the cell morphology in foamed specimens and the fracture characteristics of the specimens. Figure 5 shows representative SEM images of the fractured surfaces of the foamed and solid molded PP/LDPE blends with different amounts of AC before tensile testing. It can be seen that the foamed structure with an AC content of 0.6% in Figure 5(c) was the most uniform, with an average cell size of about 50 μm. With an increase in AC content, the number of cells decreased while the size of the cells increased. Compared to the result of the strain-at-break shown in Figure 4 and the foamed structure shown in Figure 5, it appears that there is a close relationship between the strain-at-break and the foamed structure: the more uniformly distributed the foamed structure is, the higher the ductility.

In addition, to examine the tensile properties at a higher strain rate, a tensile speed as high as 500 mm/min, which is the upper limit of the testing equipment, was also used to determine the stress–strain behavior of the different molded samples. As can be seen from Figure 6, six representative stress–strain plots were selected for comparison among samples with different amounts of AC. For the solid and foamed parts, no matter what the AC content was, yielding was first observed at approximately 10% strain. Necking took place next. It should be noted that high speed tensile tests have a different effect on samples as compared to low speed tests. In a high speed test, the necking does not have enough time to spread and cold drawing is difficult, so cracks propagate rapidly. Hence, the high-speed tensile test was also used to obtain the impact strength.[36] Similar to the tensile-impact test, it was reported to be a good way to measure the toughness of a part, although the speed of the tensile test used in this study was still lower than that of the standard tensile-impact test specified in ASTM-D1822. As a result, it can be concluded that the longer the necking lasts, the better the toughness and ductility are. Thus, from Figure 6, it can be seen that the foamed parts had better toughness and ductility than the solid ones, and that the parts with 0.6% AC performed the best.

For convenient comparison, the following integral expression of the stress–strain curve was used to describe the toughness quantitatively,

$$E = \int_0^{\varepsilon_b} \tau d\varepsilon \quad (1)$$

where τ is the apparent tensile stress, ε is the corresponding tensile strain, and ε_b is the strain-at-break. As a result, the integral value is symbolized as E with units of KJ/m^3. The result was used here simply as a direct comparison among all foamed samples. In general, the higher the integral result is, the tougher the tested sample is. According to eq. (1), the result of the six stress–strain curves are listed in Table I. As shown in Table I, the highest value calculated was 689.60 KJ/m^3, corresponding to the toughest sample with an AC content of 0.6%.

A conclusion can be drawn from the above experimental results and discussion. For the PP/LDPE 3:1 blends, the micro-foaming technology presented in this study can help to dramatically improve the strain-at-break when AC is used as the blowing agent and its content is kept around 0.6%.

Influence of the Ratio of PP and LDPE. It is well known that the mechanical behavior of PP/LDPE blends is dependent on the composition of PP and LDPE. For example, the tensile strength of the LDPE was enhanced by the addition of PP, but the elongation-at-break was drastically reduced.[4,5] According to the previous discussion, however, it is obvious that the foaming technology dramatically improved the elongation-at-break of the PP/LDPE 3:1 molded parts. So, the obvious question is: How does this affect the mechanical behavior of the foamed parts with different compositions? To keep the experimental scope manageable, the optimized AC content was fixed at 0.6%, and the results of nine different compositions of PP/LDPE foamed and solid molded parts are shown in Figures 7–11.

Figure 7 shows a direct comparison of the ductility of the representative molded samples. The tensile strength, strain-at-break, and Young's modulus with a crosshead speed of 10 mm/min are plotted against the composition as shown in Figure 8. The tensile strength and Young's modulus increased with an increase in PP content for the solid and foamed parts. This was as expected since similar observations were made by Teh[5] and Sun.[26]

Table I. Integral Results of the Stress–Strain Curves Shown in Figure 6

AC content (%)	E (KJ/m3)
0	274.32
0.5	546.91
0.6	689.60
0.8	551.81
1.0	418.40
2.0	362.74

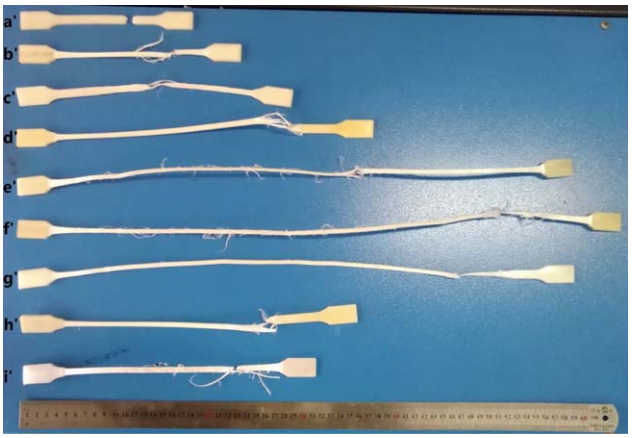

Figure 7. Pictures of the molded sample with different PP/LDPE ratios after the tensile test. The first one (a′) was the untested sample; the others (b′∼i′) were tested samples. The PP/LDPE ratios were PL31, PL01, PL13, PL12, PL11, PL21, PL31, PL41, PL51, and PL10, respectively, where the subsequent numbers denote the ratio in weight of PP/LDPE; that is, 01 means the ratio is 0:1, 11 means the ratio is 1:1, and so forth. [Color figure can be viewed in the online issue, which is available at wileyonlinelibrary.com.]

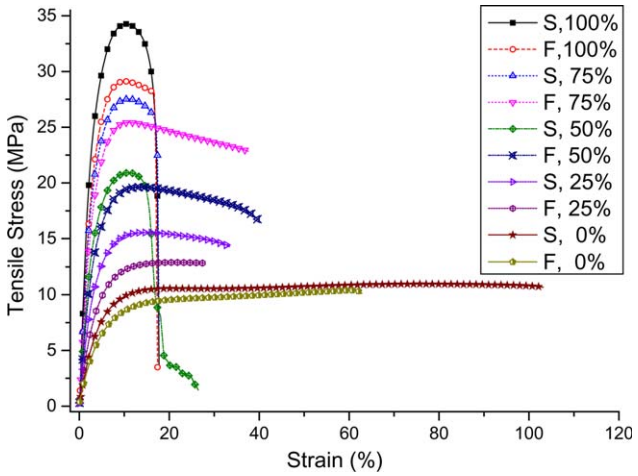

Figure 9. Tensile stress versus strain of the molded sample with different amounts of PP (tensile rate of 500 mm/min). [Color figure can be viewed in the online issue, which is available at wileyonlinelibrary.com.]

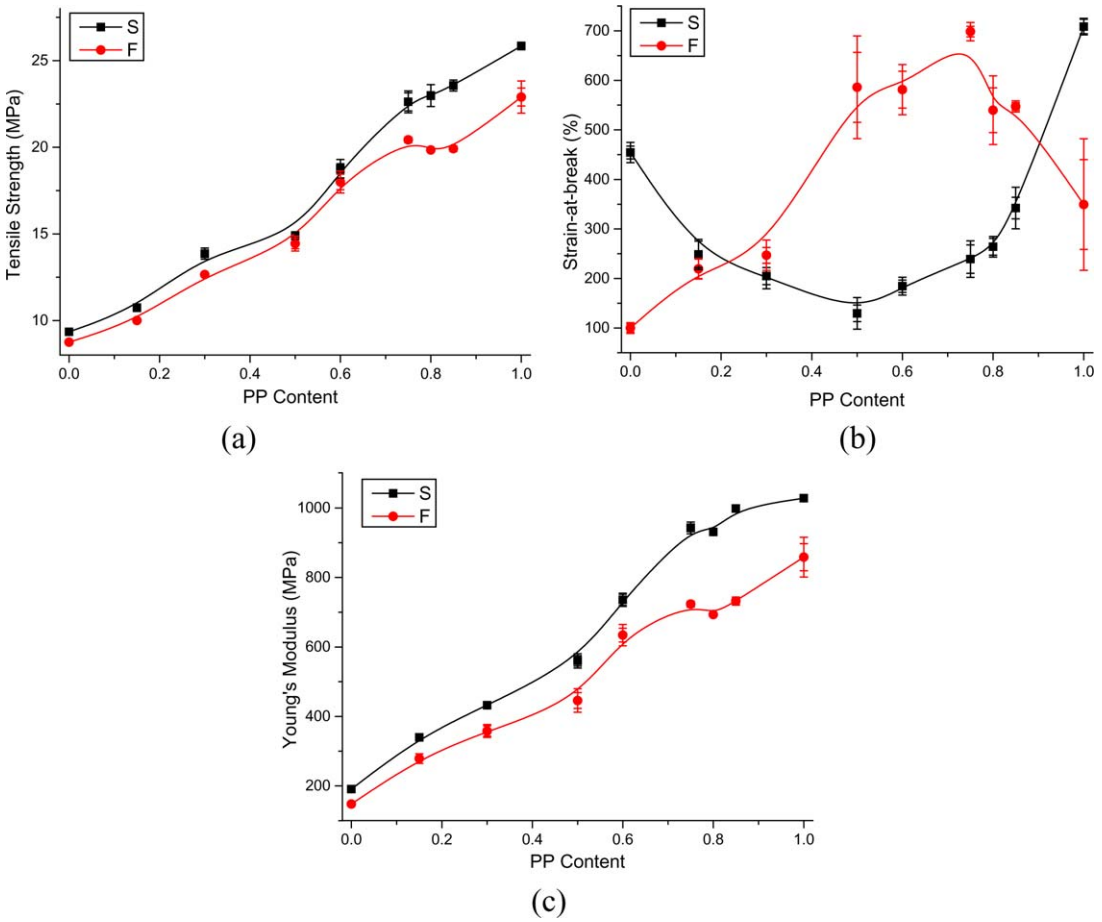

Figure 8. The (a) tensile strength, (b) strain-at-break, and (c) Young's modulus of the molded sample with different amounts of PP (tensile rate of 10 mm/min). [Color figure can be viewed in the online issue, which is available at wileyonlinelibrary.com.]

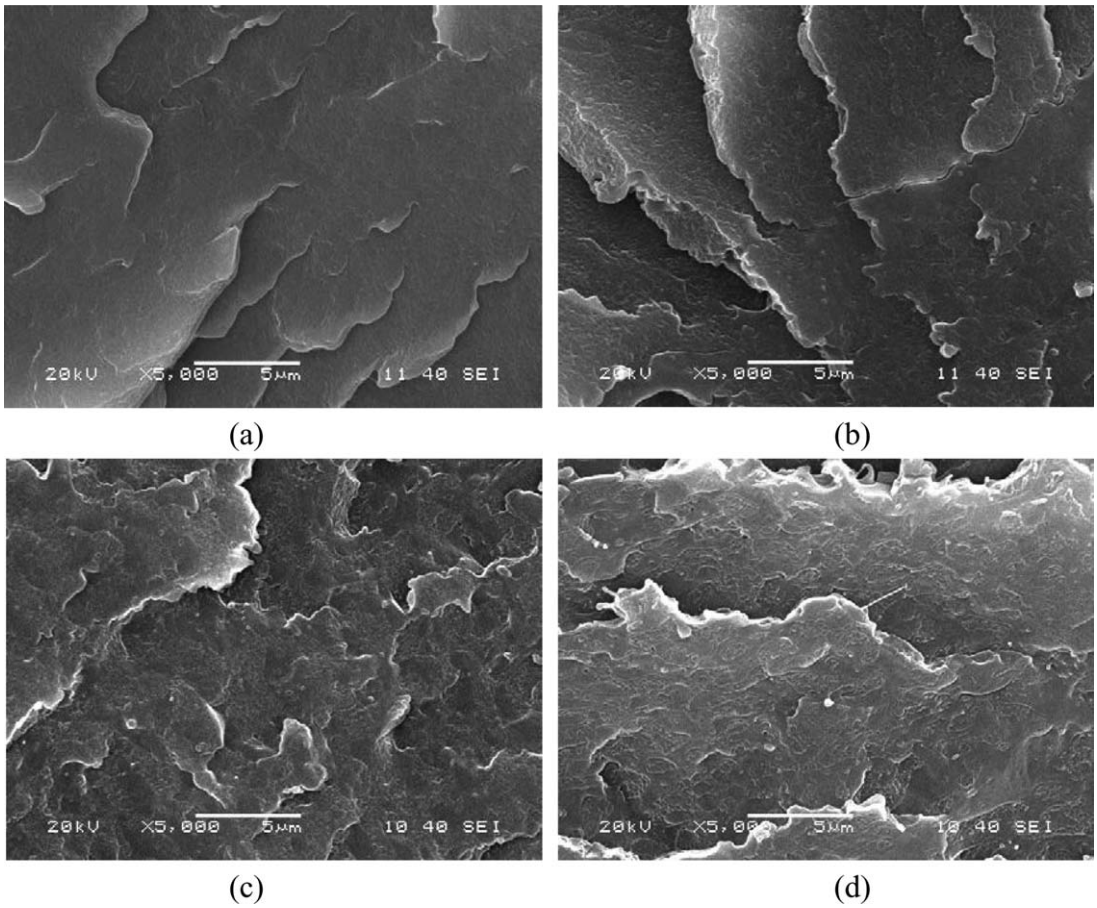

Figure 10. SEM images of the molded samples with different PP/LDPE ratios: (a) PL01, (b) PL13, (c) PL 12, (d) PL11, (e) PL21, (f) PL31, (g) PL41, (h) PL51, and (i) PL10.

However, the strain-at-break was different at different compositions and between the solid and foamed parts. For the solid parts, the strain-at-break of the poly-blends was lower than that of the homopolymers. This was in agreement with refs. 4 and 5, and was probably because of the two-phase character of the blends due to the incompatibility of LDPE and PP. However, for the foamed parts, it was just the opposite; a drastic increase in strain-at-break was observed for the foamed samples, especially when the PP content was between 50 and 85%.

The high-speed (500 mm/min) tensile test was also used to determine the toughness and ductility of the samples with different ratios of PP and LDPE. The stress–strain curves of the high-speed tensile tests are shown in Figure 9. It can be concluded that the results shown in Figure 9 are in good agreement with the results in Figure 8 where the test speed was as low as 10 mm/min. For the solid samples fabricated by the homopolymers of LDPE and PP, yielding was observed to occur at approximately 15 and 10% strain, respectively. Compared to the solid samples, the foamed specimens had a relatively low tensile strength and strain-at-break. However, for the solid samples with the poly-blends of PP and LDPE, a reduction in strain-at-break was observed to occur. Furthermore, for the foamed samples, the strain-at-break of the homopolymers was lower than that of poly-blends. In addition, a similar procedure of calculating the integral was carried out based on eq. (1), with the results listed in Table II. From Table II, it can be concluded that the foamed samples had the greatest toughness when the ratio of PP and LDPE was 3:1.

Figure 10 shows the representative SEM images of the fractured surfaces of the foamed molded PP/LDPE composites at different PP/LDPE ratios before the tensile test. As can be seen in Figure 10, the immiscibility of the PP and LDPE materials could be gradually observed with an increase in the amount of PP. In Figure 10 (b), the ratio of PP and LDPE was 1:3 and the phase dispersion was difficult to determine. With an increase in the PP content, the immiscibility became more clearly observable, as shown in Figures 10(c–h), where the particles appeared and the phase boundaries gradually became clear.

The different compatibilities at different compositions of PP and LDPE can be further characterized and verified by DSC testing of the first group (the foamed group) introduced before, the results of which are shown in Figure 11. As shown in Figure 11, although two distinct crystallization and melting peaks can be seen in the curves of all of the composites—thus indicating that the two phases of PP and LDPE are strongly immiscible—both the crystallized peak [Figure 11(a)] and the remelted peak [Figure 11(b)] of PP were shifted to the peaks

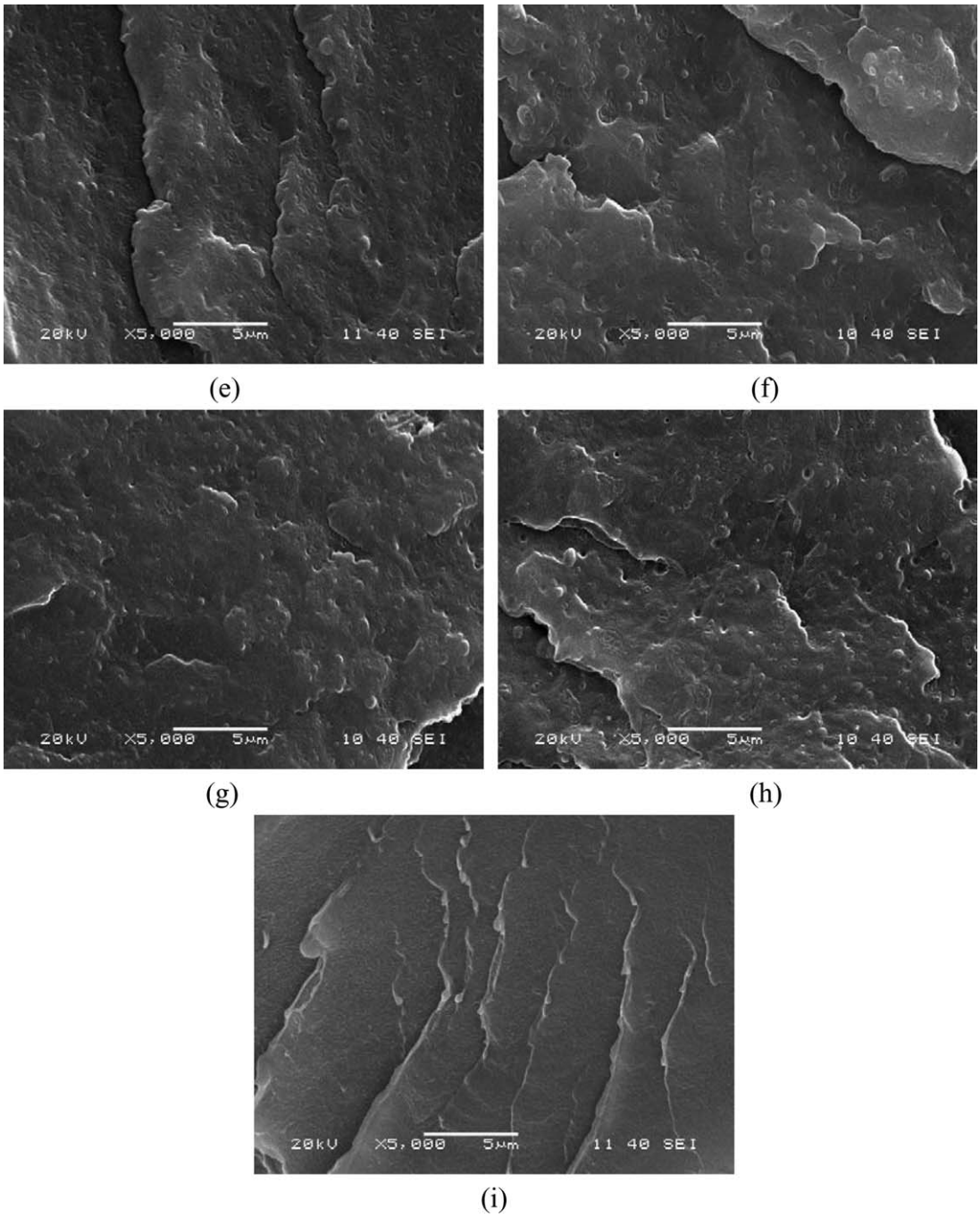

Figure 10. *Continued.*

of LDPE when the amount of PP was relative low. This suggests that the LDPE and PP were relatively miscible when the PP content was lower than 50%. It is agreement with the trend of the low strain-at-break appeared when the PP content is lower than 50%.

It can be concluded from this section that the ratio of PP and LDPE have a great effect on the compatibility of the composition, which greatly influences the foam structure and mechanical performance. In addition, the parts fabricated by blending PP and LDPE had high toughness and ductility when the PP content was in the range of 50 to 85% with an AC content of 0.6%.

Influence of Packing Pressure and Time. As discussed previously, more attention needs to be paid to the selection of processing parameters for foamed injection molding, as compared to CIM, because the decomposition of AC requires a proper range of temperature and time. Hence, the processing parameters must match the AC decomposition. It is very difficult to vary the temperature and time across a large processing window

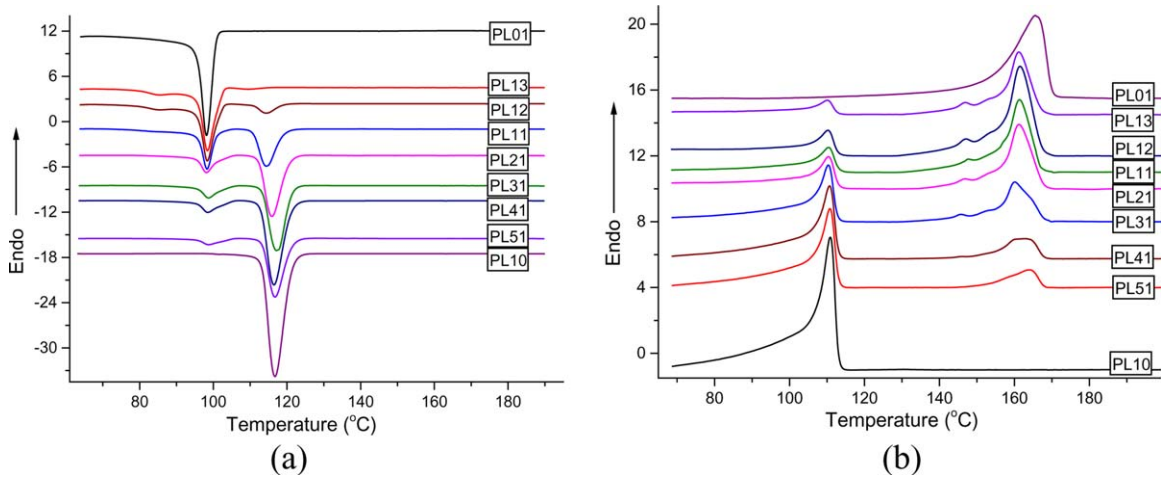

Figure 11. DSC curves (a) cooling after heating and (b) second heating of the molded samples with different PP/LDPE ratios. [Color figure can be viewed in the online issue, which is available at wileyonlinelibrary.com.]

as it involves most of the processing conditions including melt temperature, mold temperature, injection time or rate, and cooling time. However, compared with CIM, the packing stage of foamed injection molding can be varied across a reasonably wide range. On one end of the range, it can be omitted due to the expansion effect of the growth of air bubbles. On the other end of the range, it can be taken to a level as high as CIM where foaming is suppressed. It is clear that different packing pressures and times can produce different foamed structures inside of the part which will lead to different microstructures and hence different mechanical properties. As a result, the packing pressure and time need to be careful investigated to obtain a set of optimized processing parameters. In this study, the packing pressure and time in foamed injection molding were selected as 0, 10, and 30 MPa, and 0, 1, and 3 s, respectively. The 0 MPa/0 s, 0 MPa/1 s, 0 MPa/3 s, 10 MPa/0 s, and 30 MPa/0 s had almost the same effect because they all correspond to a condition where there was no substantial packing phase. Hence, there were five final different settings involved in this study: 0 MPa/0 s, 10 MPa/1 s, 10 MPa/3 s, 30 MPa/1 s, and 30 MPa/3 s. The average weights of the five conditions of foamed samples were 7.424, 7.692, 7.8576, 7.961, and 8.083 g, respectively. Compared to the solid parts, which weighed 8.219 g, the part with 30 MPa/3 s had almost no weight reduction. It can be concluded that, at this condition, the part was almost unfoamed. The part with 0 MPa/0 s had a weight reduction of 10%, and it was the lightest one.

Figure 12 shows an illustrative comparison of the ductility of the molded samples with different packing pressures and/or times, and Figure 13 shows a direct comparison of the test results of the tensile strength, elongation-at-break, and Young's modulus. Figure 14 shows the stress–strain curve for high-speed tensile testing. Also, a similar procedure of integral was carried out based on eq. (1), and the results are listed in Table 15. Figure 15 shows the foaming structure of PL31 (PP:LDPE = 3:1) parts at 0 MPa/0 s, 10 MPa/1 s, 10 MPa/3 s, 30 MPa/1 s, and 30 MPa/3 s before the tensile test. The above results indicate that the packing pressure and time greatly influenced the microstructure and mechanical performance of the samples, and that the sample with a packing pressure of 10 MPa and a packing time of 1 s obtained the best cellular structure and mechanical performance.

From the above discussions, it can be concluded that PP/LDPE super-ductile microcellular parts made with CIM with a CBA are feasible. Although the processing parameters, ratio of composition, and dosage of the blowing agent must be carefully investigated and strictly selected, the super-ductility of the foamed parts can be obtained once these conditions are optimized. In our study, an average value of 710% strain-at-break was found for the PL31 foamed sample with 0.6% AC content when the packing pressure was set at 10 MPa and the packing time was 1 s. These test results obviously exceeded those of the solid samples.

Table II. Integral Results of the Stress–Strain Curves Shown in Figure 9

PP content (%)	E (KJ/m^3, Solid)	E (KJ/m^3, Foamed)
100	400.36	341.79
75	330.62	689.60
50	261.66	559.80
25	374.33	252.10
0	855.97	463.06

Table III. Integral Results of the Stress–Strain Curves Shown in Figure 14

Packing conditions	E (KJ/m^3)
0 MPa, 0 s	298.79
10 MPa, 1 s	689.60
10 MPa, 3 s	445.54
30 MPa, 1 s	362.84
30 MPa, 3 s	280.65

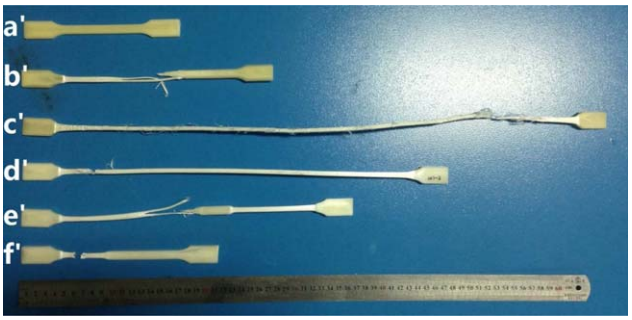

Figure 12. Optical images of the molded sample with different packing conditions before and after the tensile test. The first one (a′) is the untested sample; the others (b′∼f′) are tested samples. The packing conditions were 10 MPa/1 s, 0 MPa/0 s, 10 MPa/1 s, 10 MPa/3 s, 30 MPa/1 s, and 30 MPa/3 s, respectively. [Color figure can be viewed in the online issue, which is available at wileyonlinelibrary.com.]

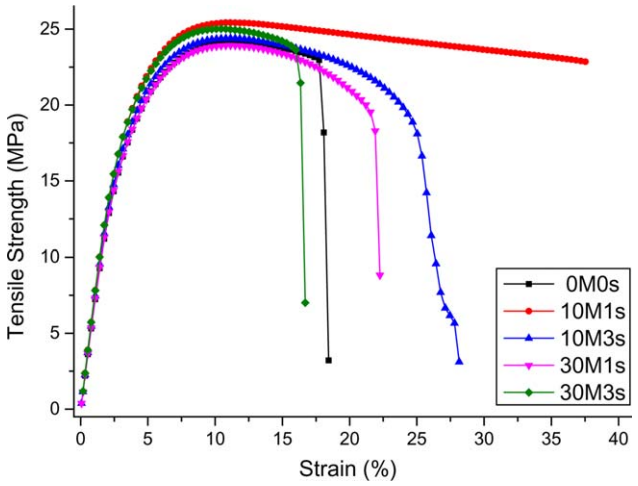

Figure 14. Tensile stress versus strain of the molded sample with different packing conditions (tensile rate of 500 mm/min). [Color figure can be viewed in the online issue, which is available at wileyonlinelibrary.com.]

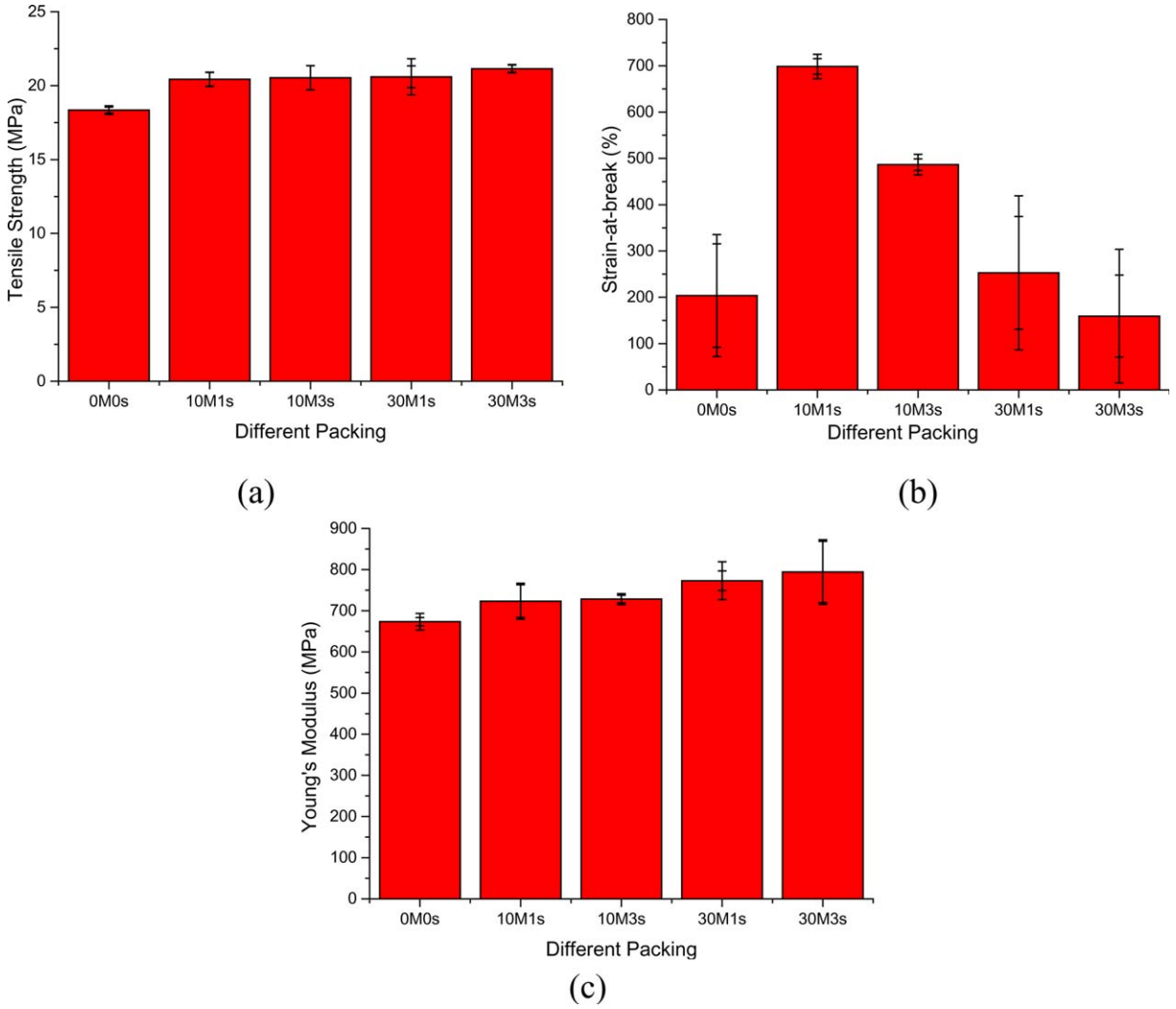

Figure 13. The (a) tensile strength, (b) strain-at-break, and (c) Young's modulus of the molded sample with different packing conditions (tensile rate at 10 mm/min). [Color figure can be viewed in the online issue, which is available at wileyonlinelibrary.com.]

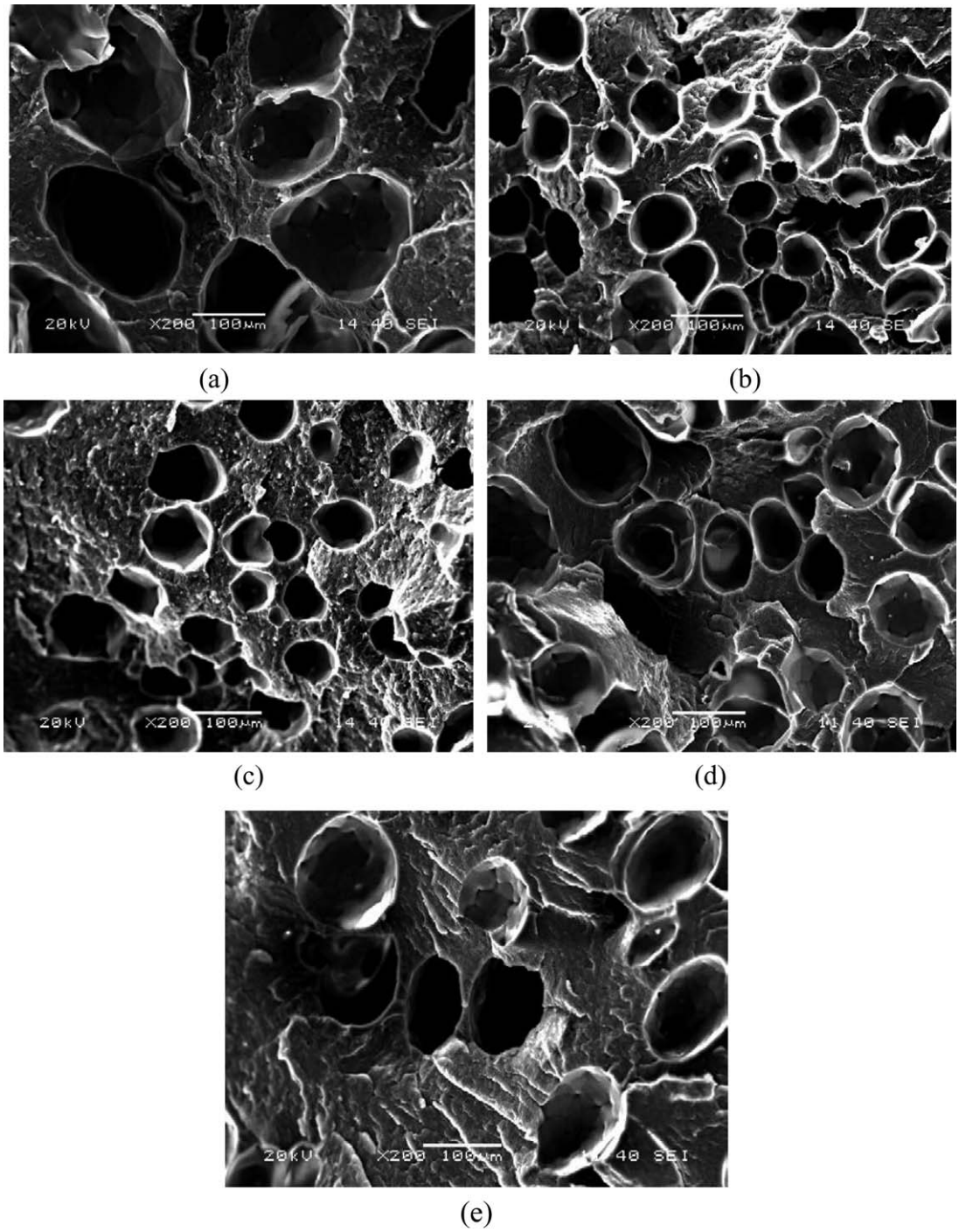

Figure 15. SEM images of the molded samples with different packing pressures and/or times: (a) 0 MPa and 0 s, (b) 10 MPa and 1 s, (c) 10 MPa and 3 s, (c) 30 MPa and 1 s, and (e) 30 MPa and 3 s.

Forming Mechanism of Fibers during the Tensile Test

For polymer blends with different compositions, the compatibility and miscibility are often viewed as two important influencing factors for their mechanical performance. Hence, the reduction of strain-at-break for the PP/LDPE blend solid parts is easily understandable and can be attributed to the two-phase character of the blends due to the incompatibility of LDPE and PP. However, the dramatically increased strain-at-break for the foamed samples remains a mystery. References 18 and 19 gave an explanation of the forming mechanism of super-ductility. Although this explanation can be viewed as reasonable, there are still some questions about the forming mechanism. For example, the explanation is deduced directly from SEM observation, and it seems to be more suitable to microcellular parts made from homopolymers. It still remains uncertain as to how the two-phase stage develops and how the cells evolve in the tensile test for the super- ductile

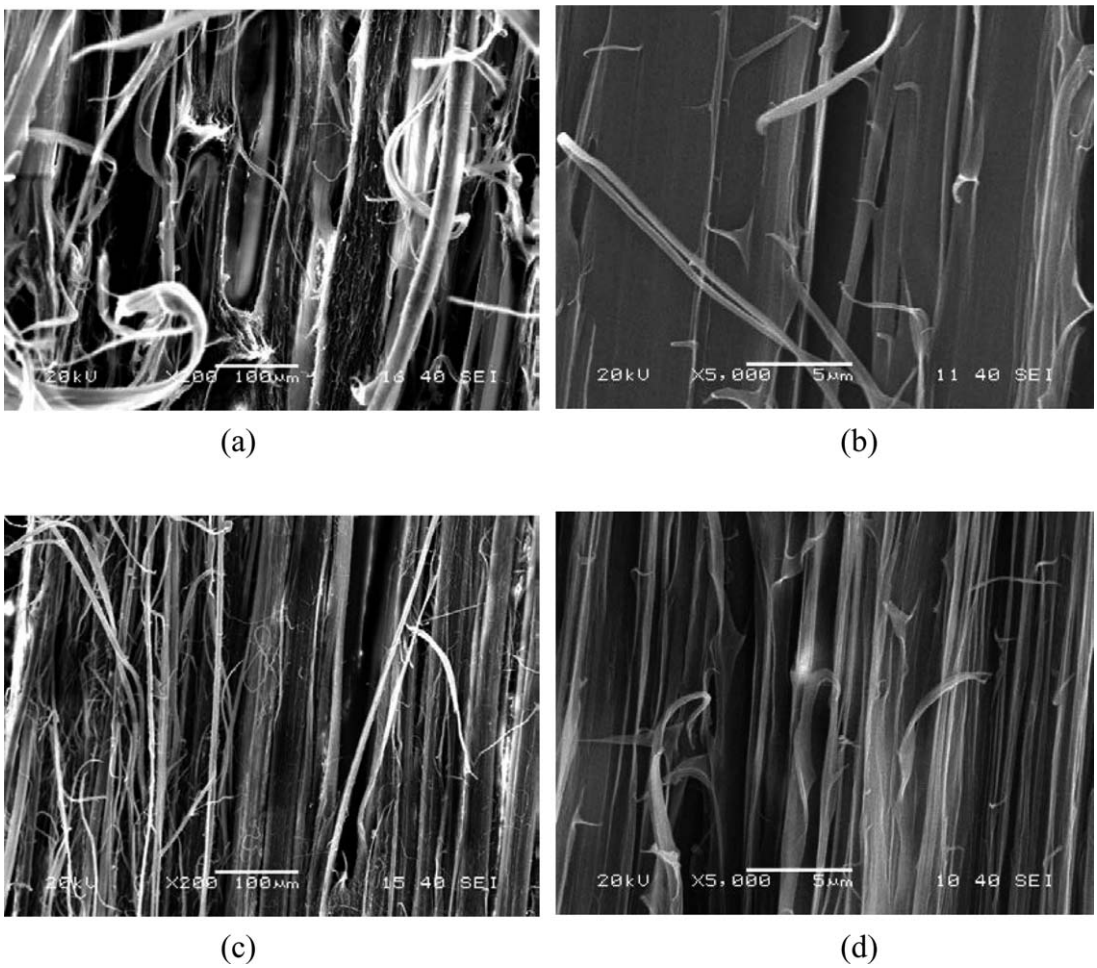

Figure 16. SEM pictures of the tensile-tested PL31 foamed sample: (a) 100% elongation, the scale bar is 100 μm; (b) 100% elongation, the scale bar is 5 μm; (c) 500% elongation, the scale bar is 100 μm; and (d) 500% elongation, the scale bar is 5 μm.

sample. As a result, it is necessary to clarify the mechanism of super-ductility more completely.

To understand the formation mechanism, the necking region of the sample tested at different elongations was also investigated by SEM, and the results are shown in Figures 16 and 17. Figure 16 shows SEM images of the micro-morphological structure of the PL31 foamed part at different elongations. A 100 and 500% elongation were carried out and are shown in Figure 16(a,c), respectively. Figure 16 (b,d) are their magnified pictures. From Figure 16, fibrillation along the tensile load direction can be observed. The foamed voids deformed simultaneously and

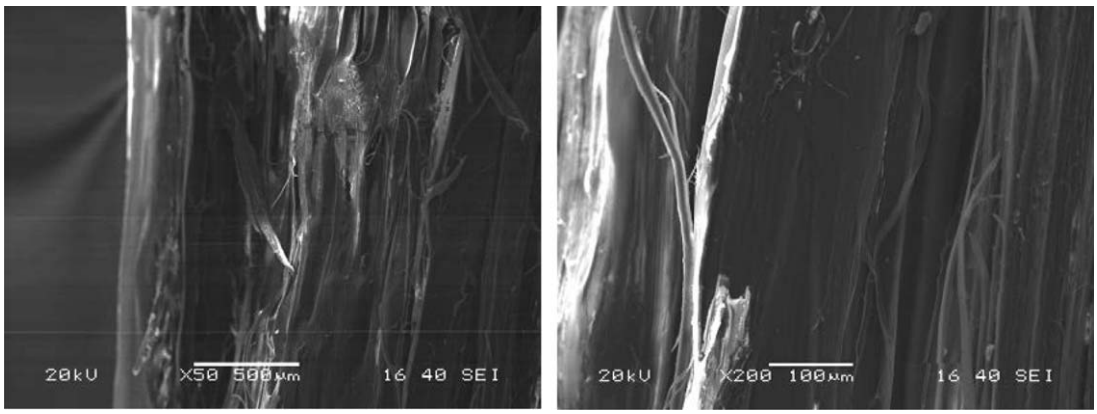

Figure 17. SEM pictures of the tensile-tested PL10 foamed sample: (a) 100% elongation, the scale bar is 500 μm, and (b) 100% elongation, the scale bar is 100 μm.

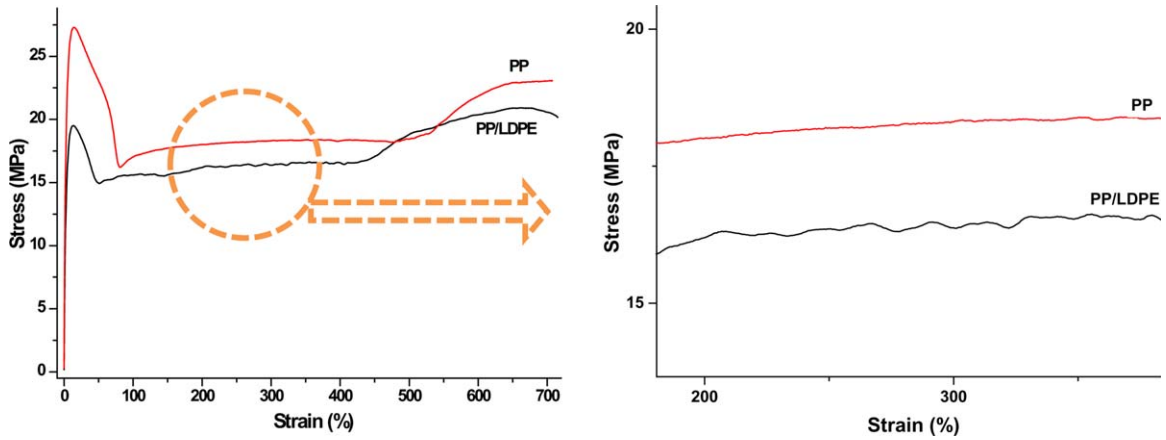

Figure 18. The stress–strain plot of the selected PP/LDPE foamed and PP solid samples. [Color figure can be viewed in the online issue, which is available at wileyonlinelibrary.com.]

functioned similarly to a solid band being split into segments. As a result, a bundle of fibrils gradually formed and divided during the tensile test. It should be noted that a similar phenomenon of deformed voids dividing into fibrils was also observed in the neat PP foamed sample; that is, the PL10 sample shown in Figure 17. Although the strain-at-break of the foamed PL10 part was lower than the solid one, necking occurred easily and 100% elongation could be seen. From Figure 17, the morphological differences between the PL31 and PL10 samples were difficult to see apart from the fewer number of bubbles in the PL10 foamed sample. The mechanism of the foamed bubbles deforming, and thus helping to divide the part into fibrils, could also be a feasible explanation for the homopolymer.

Hence, more work is still needed to understand the superductility mechanism of the foamed PP/LDPE blends. However, the stress–strain curve can give us a hint. As shown in Figure 18, for the homopolymer of the PP solid sample, yielding was observed to occur at approximately 20% strain. Necking and cold drawing continued up to several hundred percent strain, followed by ultimate rupture. This deformation behavior is typical of semi-crystalline polymers capable of undergoing chain orientation. Compared with the neat PP solid sample, the PL31 blended foamed sample had a very similar stress–strain behavior. However, after careful comparison, the stress–strain plot of the foamed PL31 parts and the solid PP parts were different during the tensile experiments. In the magnified zones shown in Figure 18(b), at 200–400% strain, the instability of the cold drawing stage of the foamed part was easily observable. The curve of the foamed sample showed an obvious, characteristic wavy curve as compared to the smooth variation of the solid PP parts. It can be assumed from Figure 18 that the instability of the stress–strain plot can be attributed to the non-uniformity of the foam structure and the PP microstructure forming micro-fibrils with a more stable structure. Furthermore, during the tensile tests, owing to the incompatibility of LDPE and PP, the LDPE can be separated from the PP and can break first when the elongation exceeds its limit.

To verify this assumption, the upper part of the ruptured fibers formed by the tensile test and the topmost part of the threadlets found at the surface of the tested PL31 sample, which are shown in Figure 19(a) and of the third group (the cold drawn foamed group) were specially taken and characterized by DSC. It must be noted that the length of the fibers and threadlets taken were only about 0.2 mm, and some separated micro-filaments could be observed when they were placed under a magnifier. The DSC results are shown in Figure 19(b), and the results were unexpected. The selected micro-filament was first heated to 170 °C, held for 1 min, and then cooled to 60 °C. After that, it was reheated to 220 °C and recooled to 60 °C. The DSC curve, as shown in Figure 19(b), compared with the DSC curves in Figure 11, indicated that the melting and

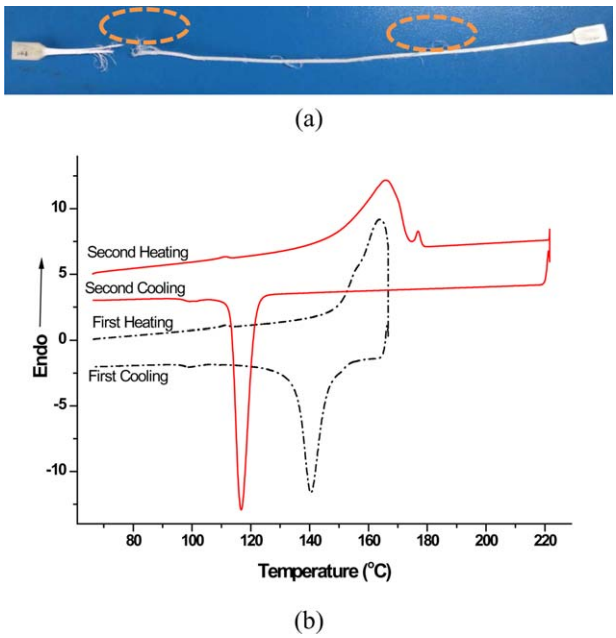

Figure 19. DSC analysis of the specified tensile-tested PL31 samples: (a) detailed location of the selected fibrils and (b) DSC test results. [Color figure can be viewed in the online issue, which is available at wileyonlinelibrary.com.]

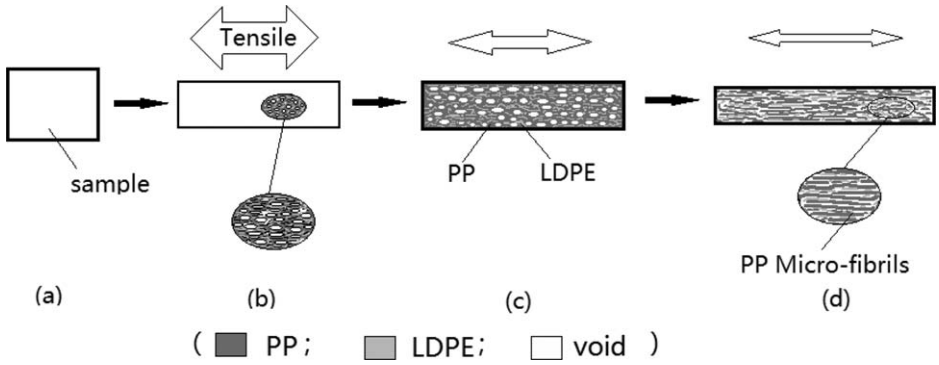

Figure 20. Model interpretation of the fiber-formation mechanism.

crystallization peaks of LDPE were difficult to find. Hence, the stretched component was mainly PP at the end of the tensile test. In addition, compared to the melting and crystallization curve and peak of neat PP, which can be found in previous work,[37] the higher temperature of the peaks also indicated that the formed microstructure was more stable.

It was concluded that the super-ductility of the PL31 samples could be attributed to the formation of PP micro-fibrils. The forming mechanism of the fibrils and micro-fibrils is illustrated in Figure 20 where, after the injection molded samples manufactured by PL31 [Figure 20(a)] were stretched, the sample gradually deformed [Figure 20(b)]. The microstructure of the sample is also shown in Figure 20(b). The phase separation between the PP and LDPE particles arose easily because of their incompatibility. With the increase in tensile strain, the stretched PP and LDPE particles continued to deform [Figure 20(c)]. The cells were connected with neighboring cells along the tensile direction, and then formed into hollow bars during stretching. As a result, the sample was separated into many fibrils due to the tensile loading. LDPE broke first with the help of the separation of the formed fibrils as the stretching gradually increased. Finally, PP continued to stretch and gradually turned into micro-fibrils, as shown in Figure 20(d).

Several *in situ* fibrillation methods have been used to improve the mechanical performance of polymer blends. For example, Leung et al.[38] studied the *in situ* fibril formation of polyethylene naphthalate (PEN) in PEN/PE and PEN/PP blends by extrusion. They found an increase in the tensile modulus of up to 100% and the tensile strength of up to one order of magnitude owing to the fibril morphology that developed during extrusion. Jiang et al.[39] found that slit die extrusion and hot stretching successfully made the dispersed polyethylene terephthalate (PET) phase in PET/HDPE blends deform *in situ* into well-defined micro-fibrils. PET micro-fibrils have a much higher axial strength and modulus than that of the HDPE matrix, which promotes the axial strength of the PET/HDPE blends. In these works, the fibrils formed mainly during polymer processing, which also had an orientation effect. As a result, the parts exhibited generally anisotropic tensile properties. However, the micro-fibrils observed in this study were not found after processing, but were actually formed during tensile testing. Hence, the manufactured part can be viewed as isotropic. Furthermore, although the "feeding and then injection" method mentioned before seems to add complexity to the operation, it can actually be solved by a simple feeding system installed on the upper end of the hopper of a CIM machine. Considering the other advantages of the chemical blowing method, such as easy storage and flexibly, it is believed that the improvement in strain-at-break based on the chemical blowing method suggested and proposed in this study—which depends on the dosage of the blowing agent, material composition, and processing conditions—is highly beneficial for academic research and industrial application. The forming mechanism of micro-fibrils is also worth further investigation for other kinds of similar polymer blends and will be the focus of our future work.

CONCLUSIONS

In this study, the feasibility and effectiveness of the fabrication of super-ductile PP/LDPE blended parts by CIM with a CBA was investigated. It was found that PP/LDPE blends have the potential to create super-ductile parts using the chemical foaming method. In particular, super-ductile foamed parts can be obtained once the packing parameter, ratio of the blends, and dosage of the blowing agent are all optimized. Compared with solid PP/LDPE blends, the injection molding foamed parts fabricated using a PP/LDPE 3:1 blend ratio with 0.6% AC exhibited greatly improved ductility when the packing pressure was set at 10 MPa and the packing time was 1 s, and also achieved a significant weight reduction of about 6.5%. It was also found that there was a close relationship between the mechanical properties and morphological structures which were greatly influenced by the packing pressure and time, ratio of the composition, and dosage of the blowing agent. The mechanism explaining the significant improvement in ductility of PP/LDPE blended foamed parts by CIM has been investigated and it is proposed that the fundamental cause was the formation of micro-fibrils in the PP phase. Accordingly, an effective way of improving toughness in the polymer blends is suggested and proposed. In addition, further investigation of the feasibility of this method and mechanism for other polymer blends was underway.

ACKNOWLEDGMENTS

The first author would like to express his gratitude to the Natural Science Foundation of Jiangsu Province (No. BK2014881) and the Priority Academic Program Development of Jiangsu Higher Education Institutions for their financial support.

REFERENCES

1. Shanks, R. A.; Li, J.; Yu, L. In Imaging and Image Analysis Applications for Plastics, A Volume in Plastics Design Library; William Andrew Inc.: New York, **1999**; p. 59.
2. Paul, D. R.; Newman, S. Polymer Blends; Academic Press: New York **1978**.
3. Robeson, L. M. *Polym. Eng. Sci.* **1984**, *24*, 587.
4. Robertson, R. E.; Paul, D. R. *J. Appl. Polym. Sci.* **1973**, *17*, 2579.
5. Teh, J. W. *J. Appl. Polym. Sci.* **1983**, *28*, 605.
6. Liang, J. Z.; Tang, C. Y.; Man, H. C. *J. Mater. Process. Technol.* **1997**, *66*, 158.
7. Rizzo, G.; Spadaro, G. *Eur. Polym. J.* **1988**, *24*, 303.
8. Dong, L. S.; Olley, R. H.; Bassett, D. C. *J. Mater. Sci.* **1998**, *33*, 4043.
9. Mourad, A. H. I. *Mater. Des* **2010**, *31*, 918.
10. Bertin, S.; Robin, J. J. *Eur. Polym. J.* **2002**, *38*, 2255.
11. Svoboda, P.; Zeng, C. H.; Wang, H.; Lee, J.; Tomasko, D. L. *J. Appl. Polym. Sci.* **2002**, *85*, 1562.
12. Nowackia, R.; Monasseb, B.; Piorkowskaa, E.; Galeskia, A.; Haudin, J. M. *Polymer* **2004**, *45*, 4877.
13. Qian, J.; Nie, K. *J. Appl. Polym. Sci.* **2004**, *91*, 1013.
14. Kim, S. H.; Ahn, S. H.; Hirai, T. *Polymer* **2003**, *44*, 5625.
15. Miltner, H. E.; Grossiord, N.; Lu, K.; Loos, J.; Koning, C. E.; Van Mele, B. *Macromolecular* **2008**, *41*, 5753.
16. Fiorentino, B.; Fulchiron, R.; Duchet-Rumeau, J.; Bounor-Legaré, V.; Majesté, J. C. *Polymer* **2013**, *54*, 2764.
17. Yousfi, M.; Livi, S.; Dumas, A.; Roux, C. L.; Crepin-Leblond, J.; Greenhill-Hooper, M.; Duchet– Rumeau, J. *J. Colloid Interface Sci.* **2013**, *403*, 29.
18. Varga, J. *J. Macromol. Sci. Part B* **2002**, *41*, 1121.
19. Malavasic, T.; Musil, V. *J. Therm. Anal.* **1988**, *34*, 503.
20. Gahleitner, M. *Prog. Polym. Sci.* **2001**, *26*, 895.
21. Ha, C. S.; Park, H. D.; Kim, Y.; Kwon, S.; Cho, W. *Polym. Adv. Technol.* **1996**, *7*, 483.
22. Fortelný, I.; Kruliš, Z.; Michálková, D.; Horák, Z. *Angew. Makromol. Chem.* **1999**, *270*, 28.
23. Fortelný, I.; Kruliš, Z.; Michálková, D.; Horák, Z. *Angew. Makromol. Chem.* **1996**, *238*, 97.
24. Barlow, J. W.; Paul, D. R. *Polym. Eng. Sci.* **1984**, *24*, 525.
25. Sun, X.; Kharbas, H.; Peng, J.; Turng, L. S. *Manuf. Lett.* **2014**, *2*, 64.
26. Sun, X.; Kharbas, H.; Peng, J.; Turng, L. S. *Polymer* **2015**, *56*, 102.
27. Saiz-Arroyo, C.; Saja, J. A.; Velasco, J. I.; Rodriguez, P. *J. Mater. Sci.* **2012**, *47*, 5680.
28. Guo, H.; Nicolae, A.; Kumar, V. *Polymer* **2015**, *70*, 231.
29. Guo, H.; Nicolae, A.; Kumar, V. *J. Polym. Sci. Part B* **2015**, *53*, 951.
30. Han, C. D.; Kim, Y. W.; Malhotra, K. D. *J. Appl. Polym. Sci.* **1976**, *20*, 1583.
31. Ruiz, J. A. R.; Vincent, M.; Agassant, J. F.; Sadik, T.; Pillon, C.; Carrot, C. *Polym. Eng. Sci.* **2015**, *55*, 2018.
32. Sauceau, M.; Fages, J.; Common, A.; Nikitine, C.; Rodier, E. *Prog. Polym. Sci.* **2011**, *36*, 749.
33. Zhou, Y. G.; Wu, W. B. Chinese Pat. 2015105574384 (**2015**).
34. Huang, M. C.; Tai, C. C. *J. Mater. Process. Technol.* **2001**, *110*, 1.
35. Galeski, A. *Prog. Polym. Sci.* **2003**, *28*, 1643.
36. Hosoda, S.; Uemura, A. *Polym. J.* **1992**, *24*, 939.
37. Zhou, Y. G.; Shen, C. Y.; Turng, L. S. *Polym. Eng. Sci.* **2010**, *50*, 1226.
38. Leung, K. L.; Easteal, A.; Bhattacharyya, D. *Compos. Part A* **2008**, *39*, 662.
39. Jiang, C. H.; Zhong, G. J.; Li, Z. M. *Macromol. Mater. Eng.* **2007**, *292*, 362.